

# A New THD Measurement Method with Small Computational Burden using a SOGI-FLL Grid Monitoring System

J. Matas, H. Martin, J. de la Hoz, A. Abusorrah, *Senior Member, IEEE*, Y.A. Al-Turki, *Senior Member, IEEE*, H. Abdalgader

**Abstract:** This paper proposes a new method for obtaining the total harmonic distortion (THD) using few math operations, a low pass filter (LPF) and a grid monitoring system able to provide the fundamental and harmonics components of the grid voltage. The method is particularly developed by using the SOGI error signal notch filter (NF) transfer function characteristics of a standard SOGI-FLL monitoring system. The method is accurate and has a small computational burden, so it is suitable for the online assessment of the grid voltage or current THD and can easily be implemented into a digital signal processor (DSP). The accuracy and transient response of the system has been analyzed, showing that they can easily be determined by the tuning of the SOGI filter and the LPF. The method also shows to be robust to grid perturbations such as voltage sags, or swells, and frequency step changes. Simulations and experimental results are provided to validate the proposed THD method. Moreover, comparison with a Fast Fourier Transform (FFT)-based THD is also presented, which shows that the proposed THD method results to be faster, more accurate and simpler than the FFT-based one.

**Index Terms-** Total harmonic distortion, THD online measurement, digital signal processor (DSP), power quality.

## I. INTRODUCTION

The THD is an important indicator to assess the quality in power systems. The THD measures the deviation of a given signal from an ideal sinusoidal pattern and can be applied to voltages and currents. In electrical systems, the supply voltage can be distorted by the interaction of consumer's nonlinear loads through the impedance of the network. The distortion can induce adverse problems such as heating of induction motors, distribution transformers and neutral conductors, the erratic operation of breakers and relays, torque pulsations in motors and generators, or the malfunction of sensitive electronic equipment. Moreover, this phenomenon can be amplified by resonance with the capacitors of power factor correction systems, which can push harmonic voltage distortion to unacceptable levels [1], [2]. To reduce these adverse effects, the IEEE standard 519-1992 provides recommended values to limit the harmonic distortion [3]. This document sets limits on voltage harmonics in low-voltage networks to 5% THD and to a 3% THD in the case of a single harmonic. These limits in practice are not enforced, so in some systems the THD content could be found to be much higher.

An online THD measurement of the grid voltage with low computational needs could be interesting in grid monitoring applications to give the ability of controlling online the distortion levels at different parts of the electrical network. It could also be used to monitor the quality of the currents absorbed by the consumer-side loads and for the detection of the use of nonlinear loads due to its specific high THD profile. For microgrids, it could be employed for the detection of nonlinear loads and to improve the quality in the grid-connected and island mode operations. Therefore, such

possibility could help in improving the quality of the power system, reducing the distortion levels.

There are few proposals in literature regarding the THD calculation, which can be grouped into frequency or time domains. In [4] a FFT and discrete Fourier transform (DFT) THD methods were proposed exploiting better the DSP accumulator capability for improving the THD calculation precision. In [5] two different THD definitions were examined in order to avoid possible ambiguity and misinterpretation in the measurement. In [6] an analytic THD calculation of non-sinusoidal signals with known Fourier coefficients filtered by band-pass filters (BPF) and using a Cauchy method of residues was proposed. In [7] a DFT variant under a non-synchronized sampling condition that approximates the fundamental frequency and improves the THD calculation is presented. In [8] a FFT and short-time Fourier transform (STFT) for calculating the THD were proposed. In [9] an analytic algebraic method for obtaining the THD in multilevel inverters considering higher order harmonics and formulating line-voltage with unequal dc-sources is proposed. In [10] a THD method using a matrix method that maps the measured harmonics into a vector of pseudo-harmonics was proposed. In [11] a THD calculation based on analog operational amplifiers to implement Fliege-BPF was proposed. This method took only into consideration the second and third harmonics and needed of manual adjustments due to mistuning of the electronic amplifiers. In [12] an analytical method for deriving the THD of the current of a single-phase multilevel inverter with an LCL filter in a grid-connected case was presented. In [13] an analytical expression for the standard THD valid for the case of using estimators with sine fitting was proposed.

In general, these proposals required of the calculation of the harmonic components of the signal using spectral analysis, which supposes a considerable computational charge to perform an online measurement of the THD and for being implemented into a DSP [4], [6]-[8]. Other proposals, [9], [11]-[13], consist on analytical solutions that provide specific formulas for the THD calculation that can be used under certain conditions and for specific converter topologies. They give insights of the causes of distortions and help to mitigate them through the design of the converter, but cannot be used for an online THD determination of arbitrary signals. Moreover, these publications provide results in which the accuracy of the obtained THD is assessed, but they do not show its dynamic behavior nor how it changes temporally as the signal distortion evolves with time.

This paper proposes a new and simple method for obtaining the THD from the fundamental and harmonic components provided by any existing adaptive notch filter (ANF) [14], adaptive BPF as those based on second order generalized integrator (SOGI) approaches [15]-[18], or PLL-

based proposals like the SOGI-PLL or EPLL [19]-[22]. The method provides the THD value but without requiring the calculation of any particular harmonic component, or performing any spectral analysis. Though the method could be applied, in general, to any grid monitoring scheme, in this work it is developed using the well-known SOGI-FLL proposal, for the sake of simplicity. The SOGI-FLL is in general a valuable tool employed to estimate the phase, frequency and amplitude of the grid voltage with low computational needs. Here, the notch filter (NF) transfer function of the SOGI error signal regarding the input signal is used for providing the grid harmonic components, while the fundamental component is obtained by means of the orthogonal outputs of the SOGI filter.

The THD is calculated using few math operations: a square of the error signal, a LPF to obtain its average, a square root and a division. The accuracy of the obtained THD relies mainly on the SOGI NF ability, which is determined by its damping factor parameter. The proposed method is simple and can help to the existing grid monitoring approaches to incorporate the THD of the grid and monitor its temporal progression through time. The method might also be used to measure the current distortion drawn by the user-side loads and for the detection of nonlinear loads, which could help the network operators to visualize and manage the grid distortion, to develop new ways of limiting their adverse effects and increase the quality of the grid.

Simulations and experimental results are provided to prove that the method is accurate and robust in face of grid voltage faults like voltage sags and phase jumps. Moreover, the method is experimentally compared with an alternative online FFT-based THD in a simple test for the detection of a 5<sup>th</sup> harmonic distortion. The FFT is implemented into a Texas Instruments (TI) DSP using a FFT optimized software library provided by this manufacturer [24]. The results show that the proposed THD achieves faster and better results than the FFT-based one, and behaves better when the grid frequency deviates from the nominal 50Hz value. The results also show that the computational load is very small compared with the FFT.

This paper is organized as follows. Section II exposes the proposed THD measurement method for being generally applied to any grid monitoring system. Section III develops the method by using the SOGI-FLL approach. A detailed analysis of the system accuracy, dynamic behavior and robustness in front of grid perturbations is provided in this section. Section IV provides experimental results for validating the proposal and compares it with an alternative FFT-based proposal. Section V exposes the conclusions of this paper.

## II. THD MEASUREMENT METHOD

Fig 1. depicts the scheme of the proposed THD measurement method, composed by few blocks: a general grid monitoring system with NF ability, a LPF and few math operations.

The method obtains the THD according the standard definition of [1] and [2] that uses the square root of the sum of the squared harmonic components of a given signal, divided by the fundamental component:

$$\text{THD} = \frac{\sqrt{\sum_h |A_h|^2}}{A_1} \cdot 100, \quad (1)$$

where  $h$  is the harmonic order and  $A_h$  is the amplitude of the

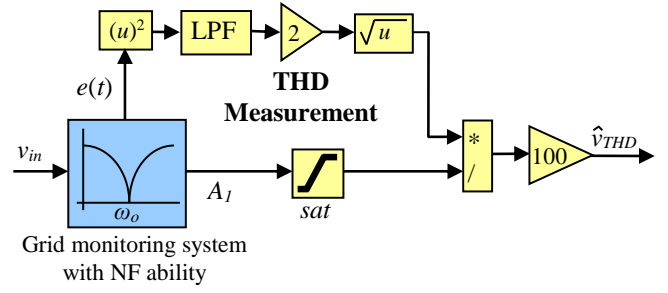


Fig. 1. Block diagram of the proposed THD measurement method.

$h$ -th harmonic component, with  $h \neq 1$ , and  $A_1$  is the amplitude of the fundamental component. The grid monitoring system should be able to provide an estimate of  $A_1$  and the rest of harmonic components contained in a given signal, named as  $e(t)$  in this case. A periodic single-phase input signal  $v_{in}$  without dc-component and only containing the odd harmonic components usually present in the grid voltage is considered for sake of simplicity, i.e.,  $h=3,5,7,\dots$ . Therefore,  $v_{in}$  can be described as

$$v_{in}(t) = A_1 \sin(\omega_i t) + \sum_h A_h \sin(h\omega_i t + \varphi_h), \quad (2)$$

where  $\omega_i$  is frequency of the grid and  $\varphi_h$  is the phase angle of the  $h$ -th harmonic component, respectively. The harmonic components can be extracted by the NF capability that some grid monitoring approaches have. Then, the signal  $e(t)$  can be identified with the second term of (2), i.e. as

$$e(t) \cong \sum_h A_h \sin(h\omega_i t + \varphi_h), \quad (3)$$

The square operation over  $e(t)$  will produce

$$e^2(t) \approx \sum_h A_h^2 \sin^2(h\omega_i t + \varphi_h) + \sum_h \sum_{k, k \neq h} A_h A_k \sin(h\omega_i t + \varphi_h) \sin(k\omega_i t + \varphi_k). \quad (4)$$

Therefore, the square operation generates the square of every harmonic in (2) plus a family of products between the harmonics. Using trigonometric identities, (4) can be expressed as

$$e^2(t) \approx \sum_h \frac{A_h^2}{2} [1 - \cos(2h\omega_i t + 2\varphi_h)] + \sum_h \sum_{k, k \neq h} \frac{A_h A_k}{2} [\cos((h-k)\omega_i t + \varphi_h - \varphi_k) - \cos((h+k)\omega_i t + \varphi_h + \varphi_k)]. \quad (5)$$

And, looking to (5), it can be seen that finally a dc-component is generated that is equal to the sum of the square of the amplitude of all the harmonic components in (3) affected by a 1/2 gain, plus a series double frequency harmonic components and plus an additional series of sinusoidal components. The last ones are components that pulsate at frequencies equal to the sum  $(h+k)$  and to the difference  $(h-k)$ , that result from the family of multiplications between harmonics in (4).

In (5) it is important to see that the relevant part corresponds to the dc-component, which is directly the sum of the square of all the harmonic components and can be used to obtain the THD of (1) without the need of complex calculations. This dc-component can be easily extracted from (5) by applying a LPF with a suitable cutoff frequency that can be designed to remove, or mitigate, the harmonic components. The LPF achieves the average value of (5), which corresponds to the dc-component and can be

expressed as

$$\rho = LPF(e^2) = \left\langle e^2 \right\rangle = \sum_h \frac{A_h^2}{2}, \quad (6)$$

where  $\langle \rangle$  represents the averaged value. The performance of the averaged value relies on the LPF cutoff frequency. Furthermore, the LPF can be of second-, third-, or  $n^{\text{th}}$ -order for the better and accurate removal of the oscillating components.

Finally, according to Fig. 1, the THD is obtained by multiplying (6) by 2 to cancel the  $1/2$  gain and by applying the square root, dividing by the fundamental amplitude  $A_1$  and multiplying by 100

$$THD = \frac{\sqrt{2\rho}}{A_1} \cdot 100. \quad (7)$$

Notice that the multiplication by 100 is only necessary to give the value in a percentage scale. In Fig. 1 the obtained THD is denoted as  $\hat{v}_{THD}$  and a saturation block is used to avoid a division by zero. The saturation is set to a small lower boundary that only has effect at the start-up transient.

Fig. 1 depicts a general scheme that might be developed using any of the several reported methods to extract the grid information based either on PLL, on adaptive notch filters (ANF), or on adaptive band-pass filters as the SOGI-FLL. However, in this paper the method is developed by using the SOGI-FLL due to its simplicity and well-known characteristics.

### III. THD DEVELOPMENT USING THE SOGI-FLL

In this section the proposed THD method is developed using the SOGI-FLL monitoring system [12]-[15], in order to check its dynamic and accuracy performance under normal and grid distorted conditions. After that, the THD accuracy regarding the NF capability of the SOGI and also the effect of the nonlinearity of the square root operator in the THD dynamic response are analyzed.

#### A. Development using the SOGI-FLL grid monitoring system

Fig. 2 depicts the block diagram of a SOGI-FLL grid monitoring system. In this figure, the SOGI consists in a frequency-adjustable resonator that is regulated with gain  $2\xi$  for having the output  $v_d$  in-phase with the input  $v_{in}$  [12]. The resonator is formed by two integrators with the particularity of providing a second output  $v_q$  in quadrature-phase with  $v_{in}$ . The FLL is a simple gradient descent algorithm that adaptively tunes the system with the frequency of  $v_{in}$  using the SOGI error  $e$  and output  $v_q$  [13]-[15].

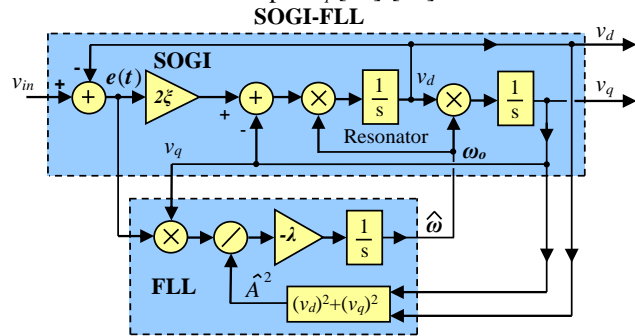


Fig. 2. SOGI-FLL block diagram.

From the input-to-output point of view, the SOGI error signal  $e(t)$  has a NF closed-loop transfer function

$$H_e(s) = \frac{e(s)}{v_{in}(s)} = \frac{s^2 + \omega_o^2}{s^2 + 2\xi\omega_o \cdot s + \omega_o^2}, \quad (8)$$

where  $\omega_o$  is the central frequency and  $\xi$  is the damping factor

that determines the NF capability. The NF behavior of  $e(t)$  is

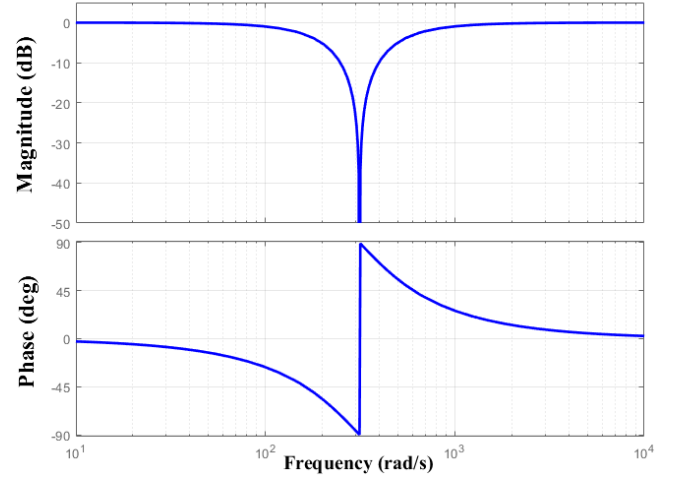


Fig. 3. Bode plot of  $H_e(s)$  for  $\zeta = 0.7$  and  $\omega_o = 2\pi 50 \text{ rad/s}$ .

used to provide the harmonic components of the grid voltage, as expressed in (3). The Bode plot of (8) is depicted in Fig. 3 for  $\zeta = 0.7$  in order to see the NF behavior.

The fundamental component of the grid voltage is estimated from the SOGI in-phase  $v_d$  and quadrature-phase  $v_q$  outputs as

$$\hat{A} = A = \sqrt{v_d^2 + v_q^2}, \quad (9)$$

where the estimated fundamental,  $\hat{A}$ , will be also denoted from now on as  $A$ . The outputs  $v_d$  and  $v_q$  have the following BPF and LPF transfer function relationship regarding the input

$$H_d(s) = \frac{v_d(s)}{v_{in}(s)} = \frac{2\xi\omega_o \cdot s}{s^2 + 2\xi\omega_o \cdot s + \omega_o^2}, \quad (10)$$

$$H_q(s) = \frac{v_q(s)}{v_{in}(s)} = \frac{2\xi\omega_o^2}{s^2 + 2\xi\omega_o \cdot s + \omega_o^2}. \quad (11)$$

The FLL estimates the grid frequency from the product between  $e$  and  $v_q$  and uses the division by the square of (9) to normalize the frequency from the grid amplitude voltage [13]-[15]. The FLL can be expressed as

$$\frac{d\hat{\omega}}{dt} = -\frac{\lambda}{A^2} \cdot e \cdot v_q, \quad (12)$$

where  $\hat{\omega}$  is the estimated frequency and  $\lambda$  is the FLL gain. Now, due to availability of the square of  $A^2$  in (9) and in Fig. 2, in this case the THD of (7) is simplified to

$$THD = \sqrt{\frac{2}{A^2} LPF(e^2)} \cdot 100 = \sqrt{2 \cdot LPF\left(\frac{e^2}{A^2}\right)} \cdot 100 = \sqrt{2 \cdot LPF(\mu)} \cdot 100$$

where  $\mu = e^2/A^2$ . And, the corresponding block diagram is shown in Fig. 4.

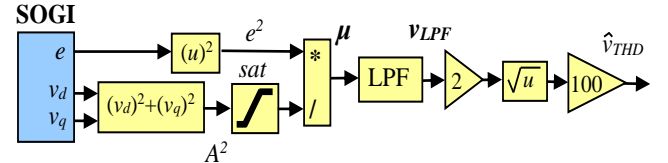


Fig. 4. THD simplified block diagram using the SOGI filter.

#### B. THD transient behavior

The system dynamic behavior for an input signal that suffers a sudden step-type THD change corresponds mainly to the dynamics of the LPF, since the harmonic perturbation goes almost unaffected to the SOGI error output and enters

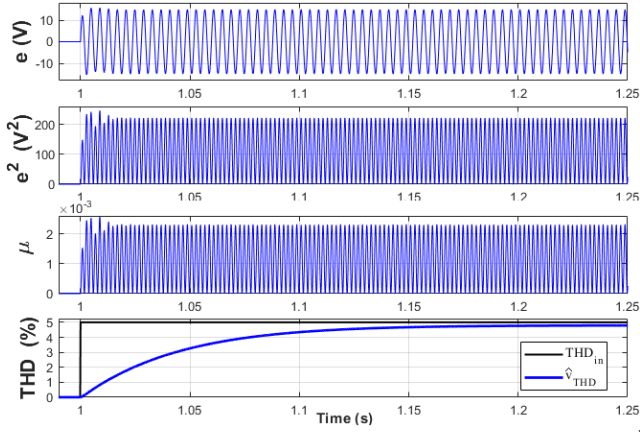


Fig. 5. THD system transient responses to a grid voltage with a 5<sup>th</sup> harmonic with 5% amplitude that appears at  $t=1s$ .

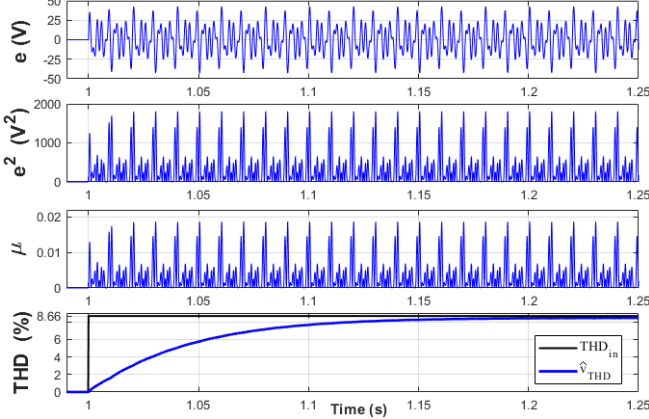


Fig. 6. THD system transient responses to a grid voltage with a combination of 5<sup>th</sup>, 7<sup>th</sup> and 11<sup>th</sup> harmonics with 5% amplitude each that appears at  $t=1s$ .

into the THD measurement method via the square operation,  $e^2(t)$ . Considering a single-phase grid voltage with a 5<sup>th</sup> harmonic step perturbation at  $t=t_0$

$$v_{in}(t) = A_1 \sin(\omega_i t) + A_5 \sin(5\omega_i t) \cdot u(t - t_0). \quad (14)$$

The perturbation goes to the LPF as

$$\mu(t) \cong \left( \frac{A_5 \cdot |H_e(j5\omega_o t)|}{A} \right)^2 \sin^2(5\omega_i t) \cdot u(t - t_0). \quad (15)$$

where  $|H_e(j5\omega_o)|$  is the SOGI NF gain at the 5<sup>th</sup> harmonic and  $\omega_o = \omega_i$ .

Fig. 5 depicts the system time response to a harmonic with 5% amplitude that appears at  $t_0=1s$ . The SOGI and LPF parameters are  $\zeta=0.7$ ,  $\omega_o = \omega_i = 2\pi 50$  rad/s,  $n=2$  and  $f_c=5$ Hz, where  $n$  is the LPF order and  $f_c$  its cutoff frequency. Note in this figure how the harmonic is transformed from bipolar in  $e(t)$ , to a unipolar signal, in  $e^2(t)$ , pulsating at high frequency, which for the LPF, in  $\mu$ , resembles like a step-like type of input perturbation. Thus,  $\mu$  is filtered by the LPF and as seen in the bottom subplot, the dynamic response is of exponential type, which corresponds to the LPF dynamics.

Additionally, Fig. 6 illustrates the time response for a combination of 5<sup>th</sup>, 7<sup>th</sup> and 11<sup>th</sup> harmonics with 5% amplitude each, appearing all at  $t_0=1s$ . Notice here that the harmonics can be seen in the  $\mu$  subplot and that the THD response still has an exponential shape. The measured THD amplitudes are 4.8% for Fig. 5 and 8.45% for Fig. 6, which implies a 4% and 2.43% measurement error, respectively. These errors are due to the SOGI NF impact to the harmonic amplitude voltages, which respectively are affected by the following gains: 0.96, 0.98 and 0.99. For Fig. 5 and Fig. 6, the measured THD settling times correspond to the LPF, i.e.  $t_s(2\%) = 4/\alpha$ , where  $\alpha = 2\pi f_c$  (rad/s).

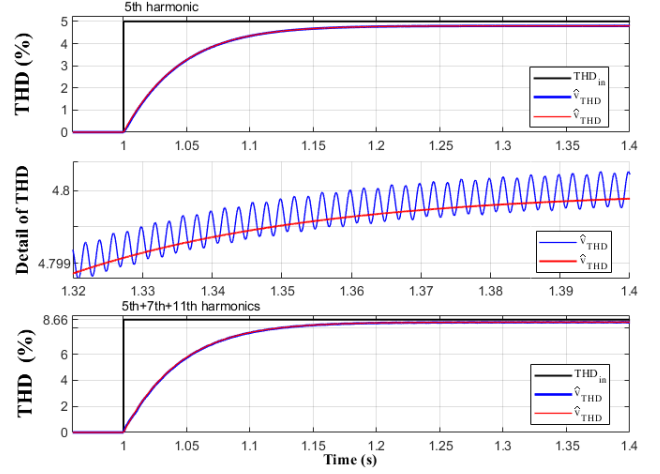


Fig. 7. THD transient response to a grid voltage with two type of harmonics with 5% amplitude each that appear at  $t=1s$ . Up: to a single 5<sup>th</sup> harmonic; Middle: Detail of the single 5<sup>th</sup> harmonic case. Bottom: to a combination of 5<sup>th</sup>, 7<sup>th</sup> and 11<sup>th</sup> harmonics.

As seen in Fig. 5 and 6, the THD dynamic follows an exponential response, which mainly is due to the LPF. The LPF averages  $\mu$  achieving the summation of the squares of the harmonic components, with each harmonic affected by the square of the SOGI NF gain. That is, at steady state, the LPF output can be expressed as

$$v_{LPF} = \frac{1}{A^2} \sum_h \frac{A_h^2 |H_{e_h}|^2}{2} \approx \frac{1}{2} \left( \frac{1}{A^2} \sum_h A_h^2 \right) \cdot \Phi = \quad (16)$$

$$= \frac{1}{2} (THD_{in})^2 \cdot \Phi$$

where  $H_{e_h} = |H_e(jh\omega_i t)|$  is the SOGI NF magnitude gain at the  $h$ -th harmonic,  $THD_{in}$  is the THD input harmonic amplitude and  $\Phi$  represents the error produced in the measurement due to the  $H_{e_h}$  NF factor. At steady state (16) goes through a multiplication by 2 followed by an  $\sqrt{\phantom{x}}$  operator, so the estimated THD is

$$\hat{v}_{THD} = THD_{in} \cdot \sqrt{\Phi} \quad (17)$$

And the dynamic behavior at  $v_{LPF}$  for a THD step-type input perturbation could be described as

$$v_{LPF}(s) = \frac{1}{2} \left( \frac{\alpha}{s + \alpha} \right)^n \Phi \cdot \frac{(THD_{in})^2}{s} \quad (18)$$

Note that in this case, the expression of the transfer function using directly the THD output  $\hat{v}_{THD}$  has not been addressed in order to avoid difficulties in the Laplace transform definition due to the square root operator. Moreover,  $\sqrt{\phantom{x}}$  has a nonlinear gain effect in a step perturbation that is not straightforward to determine and that is analyzed in detail in subsection C. Nevertheless, for assessing the dynamical behavior of  $\hat{v}_{THD}$ , Fig. 7 shows the comparison between the THD of Fig. 5 and 6, plotted in blue, with that achieved using (18) and considering the square root operator, plotted in red, i.e.  $\hat{v}_{THD}(t) = \sqrt{2 \cdot v_{LPF}(t)} \cdot 100$ . A detail is also provided in the middle subplot that proves that (18) perfectly matches the obtained responses in Fig. 5 and 6.

### C. Accuracy of the system

The measurement accuracy is determined by two factors: the SOGI NF capability for extracting harmonic components in  $e(t)$  and the distortion induced by harmonics through  $v_d$  and  $v_q$  BPF and LPF transfer functions, respectively, in the calculation of  $A$ , (9)-(11). The accuracy can be analyzed using the SOGI  $e$ ,  $v_d$  and  $v_q$  magnitude gains regarding the

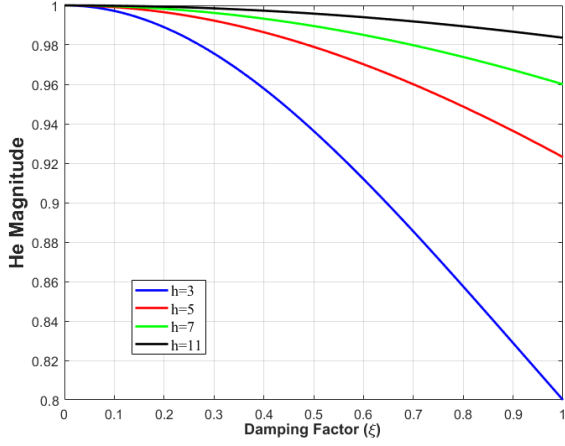


Fig. 8. Plot of  $|H_e(jh\omega_o)|$  versus  $\zeta$  for harmonic orders  $h=3, 5, 7,$  and  $11$ .

input signal, that from (8), (10) and (11) are

$$|H_e(j\omega_i)| = \left| 1 - (\omega_i / \omega_o)^2 \right| / D, \quad (19)$$

$$|H_d(j\omega_i)| = 2\xi(\omega_i / \omega_o) / D, \quad (20)$$

$$|H_q(j\omega_i)| = 2\xi / D, \quad (21)$$

Where  $D = \sqrt{(1 - (\omega_i / \omega_o)^2)^2 + (2\xi(\omega_i / \omega_o))^2}$ . And defining  $h = \omega_i / \omega_o$  can be expressed as

$$|H_e(jh\omega_o)| = |1 - h^2| / D2, \quad (22)$$

$$|H_d(jh\omega_o)| = 2\xi \cdot h / D2, \quad (23)$$

$$|H_q(jh\omega_o)| = 2\xi / D2. \quad (24)$$

where  $D2 = \sqrt{(1 - h^2)^2 + (2\xi \cdot h)^2}$ .

Regarding  $e(t)$ , the magnitude of (22) can be simplified to  $|H_e(jh\omega_o)| \cong 1$  for  $h \geq 5$ , since  $h^2 \gg 2\xi h$  for  $h \geq 5$ . This means that the THD is quite accurate for  $h \geq 5$  and that the THD method is appropriate then for three-phase systems. However, for  $h < 5$  the harmonics are significantly attenuated for increasing values of the SOGI damping factor  $\zeta$ . This fact can be seen in Fig. 8 in which the relationship between  $|H_e(jh\omega_o)|$  in (20) and  $\zeta$  is plotted for  $h=3, 5, 7,$  and  $11$ .

In Fig. 8 the highest  $|H_e|$  attenuations are obtained also for the highest  $\zeta$ . So, for  $\zeta=1$ , the 3<sup>rd</sup>, 5<sup>th</sup>, 7<sup>th</sup> and 11<sup>th</sup> harmonics will be affected by the attenuation factors 0.2, 0.08, 0.04 and 0.0164, respectively. However,  $|H_e|$  can be adjusted to a desired level by simply reducing  $\zeta$ . For instance, using Fig. 8 or (22), for  $h=5$  the attenuation can be limited to only 1% by choosing  $\zeta=0.34$ .

The accuracy can further be analyzed assuming a grid voltage with a single harmonic component

$$v_{in}(t) = A_1 \sin \theta + A_h \sin \theta_h, \quad (25)$$

where  $\theta = \omega t$  and  $\theta_h = h\omega t + \varphi_h$  are the phases of the fundamental and harmonic components, respectively. Assuming that the SOGI is tuned to the input frequency ( $\omega_o = \omega_i$ ), the outputs  $e$ ,  $v_d$  and  $v_q$  are

$$e(t) = A_h |H_e| \sin \theta_{he} \quad (26)$$

$$v_d(t) = A_1 \sin \theta + A_h |H_d| \sin \theta_{hd}, \quad (27)$$

$$v_q(t) = -A_1 \cos \theta - A_h |H_q| \cos \theta_{hd}, \quad (28)$$

where  $|H_e| = |H_e(jh\omega_o)|$ ,  $|H_d| = |H_d(jh\omega_o)|$ ,  $|H_q| = |H_q(jh\omega_o)|$ ,  $\theta_{he} = h\omega t + \psi_e$ ,  $\theta_{hd} = h\omega t + \psi_d$ ,  $\psi_e = \angle H_e(jh\omega_o)$  and  $\psi_d = \angle H_d(jh\omega_o)$ . And, the square of  $A$  in (9) can be expressed as

$$A^2 = A_1^2 + A_h^2 |H_d|^2 \sin^2 \theta_{hd} + A_h^2 |H_q|^2 \cos^2 \theta_{hd} + 2A_1 A_h |H_d| \sin \theta \sin \theta_{hd} + 2A_1 A_h |H_q| \cos \theta \cos \theta_{hd} \quad (29)$$

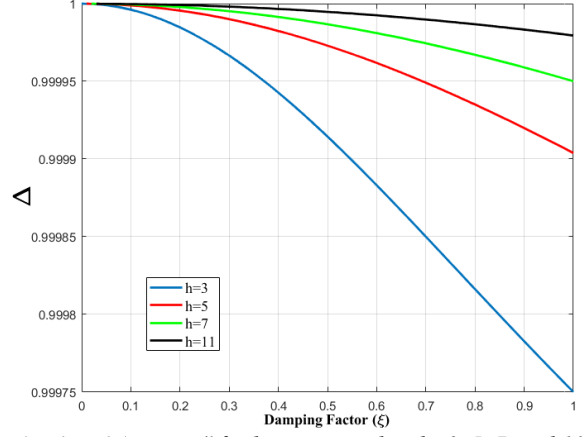


Fig. 9. Plot of  $\Delta$  versus  $\zeta$  for harmonic orders  $h=3, 5, 7,$  and  $11$ .

which, considering that (24) can be simplified to  $|H_q| = |H_d|/h$  and using trigonometric identities, leads to

$$THD = \sqrt{2 \left\langle \frac{\frac{1}{2} A_h^2 |H_e|^2 (1 - \tilde{q})}{A_1^2 + j + \tilde{r} + \tilde{u}} \right\rangle} \cdot 100, \quad (30)$$

where  $\langle \rangle$  is the average and  $\sim$  indicates an oscillating component and  $\tilde{q} = \cos 2\theta_{he}$ ,  $j = \frac{1}{2} A_h^2 |H_d|^2 \frac{1 + h^2}{h^2}$ ,

$$\tilde{r} = \frac{1}{2} A_h^2 |H_d|^2 \frac{1 - h^2}{h^2} \cdot \cos(2\theta_{hd}),$$

$$\tilde{u} = A_1 A_h |H_d| \frac{1}{h} [(1 + h) \cdot \cos(\theta_{hd} - \theta) + (1 - h) \cdot \cos(\theta_{hd} + \theta)]$$

And, knowing that the average of the oscillating components is zero, (30) can be simplified to

$$THD = \sqrt{\frac{A_h^2 |H_e|^2}{A_1^2 + j}} \cdot 100 \quad (31)$$

which can be put in the form

$$THD = \sqrt{\frac{A_h^2 |H_e|^2}{A_1^2}} \cdot \frac{1}{\sqrt{1 + \frac{1}{2} \left( \frac{A_h}{A_1} \right)^2 |H_d|^2 \frac{1 + h^2}{h^2}}} \cdot 100 = \sqrt{\frac{A_h^2 |H_e|^2}{A_1^2}} \cdot \Delta \cdot 100 \quad (32)$$

$$\text{being } \Delta = \left( \sqrt{1 + \frac{1}{2} \left( \frac{A_h}{A_1} \right)^2 |H_d|^2 \frac{1 + h^2}{h^2}} \right)^{-1}.$$

Consequently, the accuracy is affected by a term  $\Delta$  that is determined by the relationship  $A_h/A_1$ ,  $|H_d|$  and  $h$ . This term has a small impact since the product  $(A_h/A_1)^2 |H_d|^2 \ll 1$  and then it could be obviated in (32). However, Fig. 9 plots the relationship between  $\Delta$  and  $\zeta$  for  $h=3, 5, 7,$  and  $11$  with 5% amplitude with the aim to see its real impact on (32).

Fig. 9 shows that in the worst case  $\Delta$  will impact the THD by an attenuation that is below  $2.5 \cdot 10^{-4}$ , for  $h=3$ . Then,  $\Delta$  can be neglected and it can be assumed that the accuracy is mainly determined by  $|H_e|$ , i.e. the NF capabilities of the SOGI filter, which can be adjusted by  $\zeta$ .

Finally, Fig. 10 shows the THD response for  $\zeta=0.34$  (1% of error at a 5<sup>th</sup> harmonic, see Fig. 8) for a simulation in which a 5<sup>th</sup> harmonic appears at  $t=1s$ , a 7<sup>th</sup> harmonic appears later at  $t=1.5s$  and 11<sup>th</sup> harmonic at  $t=2s$ , which can be visually seen as a staircase perturbation. Each harmonic is of

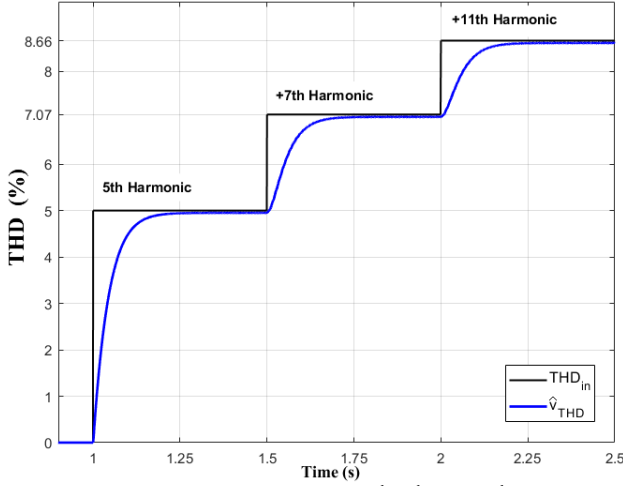


Fig. 10. THD transient response for a 5<sup>th</sup>, 7<sup>th</sup> and 11<sup>th</sup> harmonics of 5% amplitude each. First a 5<sup>th</sup> harmonic appears at  $t=1s$ , then a 7<sup>th</sup> at  $t=1.5s$  and an 11<sup>th</sup> at  $t=2s$ .

5% amplitude. In Fig. 10, the measured THD for the 5<sup>th</sup> harmonic is 4.95% with an 1% error, as expected. The THD for the combination of the 5<sup>th</sup> and 7<sup>th</sup> harmonics is 7.02%, which supposes a 0.72% error. And for the 5<sup>th</sup>, 7<sup>th</sup> and 11<sup>th</sup> combination the THD is of 8.60%, which is an error of 0.70%.

#### D. Impact of the square root nonlinear operator in the dynamic response

The square root  $Y=\sqrt{X}$ , is a nonlinear operator that is plotted in Fig. 11 for the interval  $0 \leq X \leq 100$ . As can be seen in the enlargement subplot in the lower right corner of this figure, the square root function presents a high slope for the arguments closer to zero. Nevertheless, the slope progressively decreases as the arguments grow. Therefore, the square root dynamically modifies the gain of the THD measurement system at the event of an input step harmonic perturbation. As a result, the step-up and step-down THD transient responses are unequally affected by this gain.

This fact can be seen in the lower subplot of Fig. 12 that depicts the THD transient response to a single 5<sup>th</sup> harmonic with 5% amplitude considering the square root operator ( $\hat{v}_{THD}$  signal, in blue line) and not considering it ( $\hat{v}_{THDx}$  signal, in red line). The last one has been scaled in gain and named  $\hat{v}_{THDx}$  in order to match the same steady state value of  $\hat{v}_{THD}$  and allow their comparison. In this figure, at the step-up at  $t=1s$ , for the initial small values of  $THD_{in}$  the calculated  $\hat{v}_{THD}$  grows up faster than  $\hat{v}_{THDx}$  due to the square root high gain. Nevertheless, the gain slows down as  $THD_{in}$  increases, resulting in similar settling times for both signals.

On the other hand, at the step-down at  $t=1.5s$ , as  $THD_{in}$  begins to decrease, the signal at  $\hat{v}_{THD}$  reduces at a progressively slower rate, due to the square root operator high gain for low input values, leading to significant differences in their settling times. So, the square root produces a small advancing effect at the step-up and a strong delaying effect at the step-down transient response, which can be clearly seen in the lower subplot. However, this asymmetrical phenomenon disappears for step transients starting from THD levels that are away from zero, which can be seen in the upper subplot of Fig. 12. Note in this case that there is a permanent 5<sup>th</sup> harmonic with 5% amplitude and a transient to an 8.66%. The THD step perturbation happens at  $t=1.5s$  and disappears at  $t=2s$ . Notice that there is a small difference in this case between  $\hat{v}_{THD}$  and  $\hat{v}_{THDx}$ . And that the

response at the step-up and step-down transients tend to be

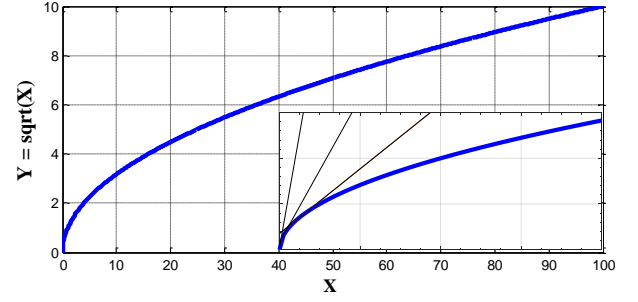


Fig. 11. Plot of the square root function, and enlargement for the arguments closer to zero, showing the initial high slopes.

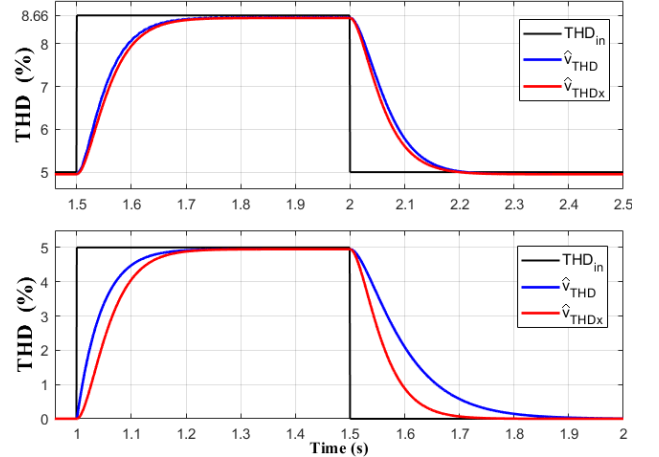


Fig. 12. Response to two different THD step changes: up) from 5% to 8.66% at  $t=1.5s$  and then back to 5% at  $t=2s$ ; down) from 0% to 5% at  $t=1s$  and then back to 0% at  $t=1.5s$ . In blue: THD output. In red: Scaled THD before square root operation.

symmetrical and that  $\hat{v}_{THD}$  is more close to  $\hat{v}_{THDx}$ . Note in the lower subplot of this figure that the square root advances a little bit (0.025s) the step-up response and strongly delays (0.14s) the step-down one.

#### E. Response to frequency step changes and voltage sags

The perturbations of the grid like voltage sags and frequency step changes reach the THD through the relation  $\mu=(e/A)^2$  in (13). This relationship can be addressed by viewing first the time derivative of the SOGI error, which from Fig. 2 can be defined as

$$\dot{e} = \dot{v}_i - \dot{v}_d = \dot{v}_i - \hat{\omega} \cdot (2\xi \cdot e - v_q), \quad (33)$$

where  $\hat{\omega}$  is the FLL estimated frequency. Hence, assuming steady state conditions and that there is a frequency step perturbation in the grid, i.e.  $v_i = A_1 \sin[(\omega_i + \Delta\omega)t]$ , being  $\Delta\omega$  the frequency perturbation step size, (31) becomes

$$\dot{e} = (\omega_i + \Delta\omega)A_1 \cos[(\omega_i + \Delta\omega)t] - \hat{\omega} \cdot (2\xi \cdot e - v_q), \quad (34)$$

which determines the perturbation dynamics in  $e(t)$ . Moreover, the dynamics of  $\hat{\omega}$  can be considered as is described in [23] as

$$\hat{\omega}(s) = \frac{\lambda/2}{s^2 + \xi\omega_n \cdot s + \lambda/2} \Delta\omega(s) \quad (35)$$

where  $\omega_n=2\pi 50\text{rad/s}$ . On the other hand, through the time derivative of (9) and denoting now  $A$  as the estimate of  $A_1$ , the perturbation effect in  $A$  can be seen as

$$\frac{dA}{dt} = \frac{v_d \cdot \dot{v}_d + v_q \cdot \dot{v}_q}{(v_d^2 + v_q^2)^{1/2}} = \frac{v_d \cdot \dot{v}_d + v_q \cdot \dot{v}_q}{A}, \quad (36)$$

which according (33),  $\dot{v}_d = \hat{\omega} \cdot (2\xi \cdot e - v_q)$  and  $\dot{v}_q = \hat{\omega} \cdot v_d$  gives

$$\frac{dA}{dt} = \frac{2\xi}{A} \hat{\omega} \cdot v_d \cdot e. \quad (37)$$

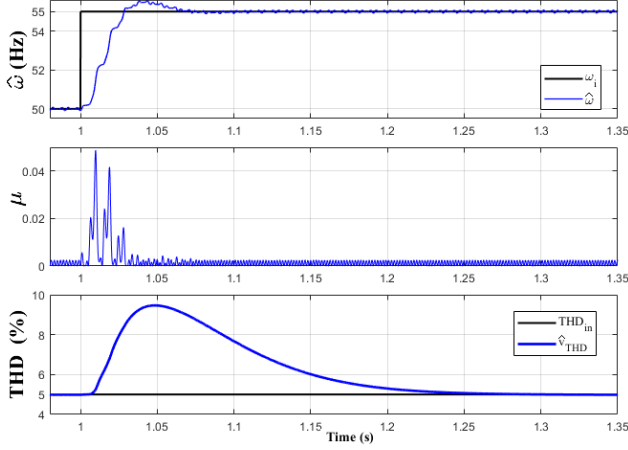


Fig. 13. Transient responses obtained for a frequency step perturbation from 50Hz to 55Hz at  $t=1s$ . The grid has a permanent 5<sup>th</sup> harmonic with 5% amplitude. Up: SOGI-FLL estimated frequency. Middle:  $\mu$ . Down: THD.

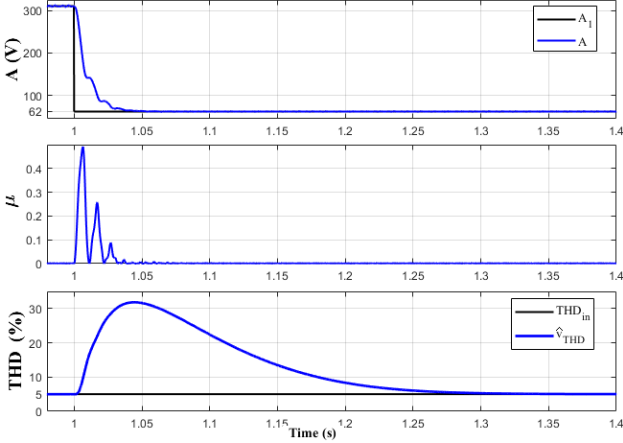


Fig. 14. Transient responses obtained for an 80% depth voltage sag perturbation at  $t=1s$ . The grid has a permanent 5<sup>th</sup> harmonic with 5% amplitude. Up: SOGI-FLL estimated amplitude voltage. Middle:  $\mu$ . Down: THD.

Table I. THD measured peak amplitude due to frequency step perturbations of different sizes.

Frequency step size	2Hz	4Hz	6Hz	8Hz	10Hz
THD perturbation amplitude (THD-5%)	0.93	3.14	5.86	8.82	11.90

Table II. THD measured peak amplitude due to voltage sags of different depths.

Voltage sag depth size	20%	40%	60%	80%
THD perturbation amplitude (THD-5%)	2.01	7.18	14.81	26.82

So,  $A$  will be also perturbed by  $\hat{\omega}$  and by  $e = v_m - v_d$ . Therefore, due to the combination of (34) and (37),  $\mu$  is not straightforward to analyze, but the impact of the perturbation can be assessed using simulations. To this aim, Fig. 13 shows the response to a perturbation from 50Hz to 55Hz at  $t=1s$  for a grid with a permanent 5<sup>th</sup> harmonic of 5% amplitude. The SOGI-FLL and LPF parameters were:  $\lambda=55 \cdot 2\pi 50 \text{ rad/s}^2$ ,  $\xi = -0.34$ ,  $n = 2$  and  $f_c = 5 \text{ Hz}$ , respectively, which have been designed for achieving a 1% error at a 5<sup>th</sup> harmonic and a 10% overshoot in the transient response.

As can be seen, in  $\mu$  the perturbation causes a burst of

pulses that the LPF averages, generating an impulsive-like transient response in the THD. This burst is mainly produced by the quadratic operation over  $e$  that turns positive the negative cycles of the error signal.

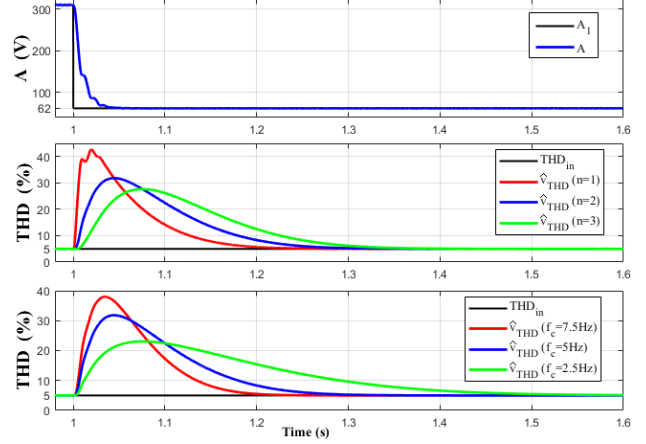


Fig. 15. THD transient responses for an 80% depth voltage sag perturbation at  $t=1s$ . The grid has a permanent 5<sup>th</sup> harmonic with 5% amplitude. Up: SOGI-FLL estimated amplitude voltage. Middle: THD for different LPF orders,  $n=1, 2$  and 3. Down: THD for and different cutoff frequencies,  $f_c=7.5, 5$  and  $2.5 \text{ Hz}$ .

Fig. 14 depicts the transient response to an 80% depth voltage sag at  $t=1s$ . Notice that the same behavior is achieved than in the previous figure, but with a higher THD peak. As a consequence, in both cases, the THD is perturbed transiently with a transient dynamic that is due to the LPF.

The peak size of these perturbations was measured for different frequency and voltage sags with different step sizes and depth levels regarding the 5% that is permanently being measured. Tables I and II summarize these data, which show that the impact of the perturbation in the THD increases naturally with the perturbation magnitude. It can be concluded that for the frequency case, the THD impact follows a quadratic input-to-output relationship as  $y=a_2x^2+a_1x+a_0$ , with  $a_2=0.0035$ ,  $a_1=0.97$  and  $a_0=-1.2$ . And for the voltage sag, the THD impact can be approximated by a cubic law as  $y = b_3x^3+b_2x^2+b_1x+b_0$ , being  $b_3=4 \cdot 10^{-5}$ ,  $b_2=-0.0017$ ,  $b_1=0.25$  and  $b_0=-2.6$ .

The THD impact can be generally mitigated by adjusting the LPF parameters. In the frequency case, it can also be reduced minimizing the frequency overshoot by reducing the FLL gain. Fig. 15 illustrates this fact by showing the THD response for the voltage sag case when different filter orders  $n$ , and cutoff frequencies  $f_c$ , are used.

As seen in Fig. 15, an increase in  $n$  or decrease in  $f_c$  helps to reduce the THD perturbation. The most effective parameter is  $f_c$ , which reduces more the impact on the THD, but producing a longer transient response. The increase in  $n$  helps to reduce the impact, but the reduction capacity is lower for  $n>3$ .

#### IV. EXPERIMENTAL RESULTS

Experimental results were first obtained using a Chroma 61501 single-phase programmable AC power source, an analog sensing-board prototype wired to a Texas Instruments (TI) Concerto F28M35H52C1 DSP control board, and a personal computer with Code Composer Studio software environment from TI. The Concerto DSP is a dual core processor that has an ARM Cortex-M3 and a TMS320C28x inside the same chip. The ARM processor is devoted to communications purposes that are not used for this work.

The TMS320C28x is a 32-bit floating point processor that runs at 150MHz clock speed and has 512kb Flash memory. Both processors have a shared RAM memory of 64kb. The sensing-board included a 4-channel and 12-bit DAC7564

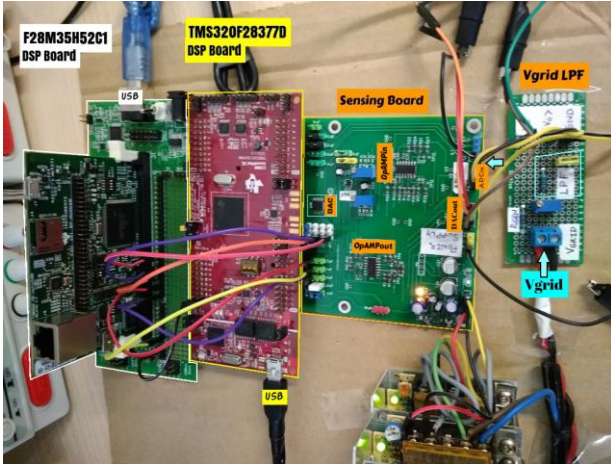


Fig. 16. Experimental setup using two DSP boards and an analog sensing board.

digital-to-analog (DAC) chip wired to the DSP control board using a Serial Peripheral Interface (SPI) communication protocol. The DAC allowed to display up to four DSP internal variables in real-time within a 0 to 3V output voltage window. An R-C analog LPF with a 1500Hz cutoff frequency is used in the sensing of the grid voltage to avoid to introduce in the measurement the high frequency switching noise of the AC power source. Moreover, a digital high-pass filter (HPF) and a LPF with 1Hz and 1500Hz cutoff frequencies, respectively, were also used in order to avoid the influence of subharmonics and of the DSP high sampling frequency. The experimental results obtained by using the Concerto board are showed in Figs. 17 to 24.

The comparative experimental results were obtained by measuring the harmonic components using a FFT and by using a TI's TMS320F28377D 200Mhz 32-bit floating point second-DSP's board. The TMS320F28377D has the same 512kb Flash memory capability than the Concerto board. However, it has more Ram memory, till 172kb. This control board is necessary to run properly the FFT routine provided by TI's software library [24], since this routine did not run in the Concerto board due to insufficient Ram memory capability. This board has a three-channel 12-bit DAC peripheral embedded inside the DSP processor. Fig. 16 depicts a picture of all these boards together. Therefore, the comparison is made from the simultaneous results obtained by the first and second DSP boards. In the comparison, the proposed THD method was implemented in the first DSP, while the FFT-based one was implemented in the second DSP. The comparative results are depicted in Figs. 25 to 29. For both boards, the sampling frequency was 20kHz and the SOGI-FLL and the THD measurement diagram block were discretized and implemented using the Backward Euler method.

#### A. Results of the proposed THD measurement method

A periodic 5<sup>th</sup> harmonic perturbation of 5% amplitude was programmed in the AC power source with a 220V(rms)/50 Hz fundamental voltage. Fig. 17 shows the AC power source voltage in channel 1, the obtained THD measurement in channel 2 and a step 5% THD artificial signal in channel 3 generated to contrast with the measurement. The SOGI and

LPF parameters were  $\zeta=0.7$ ,  $\omega_o=2\pi 50\text{rad/s}$ ,  $n=2$  and  $f_c=5\text{Hz}$ . The signals in channels 2 and 3 were amplified to fit them to the 3V DAC output window, so the vertical axis gains were 200mV/div, which in this case corresponded to 1.66%/div.

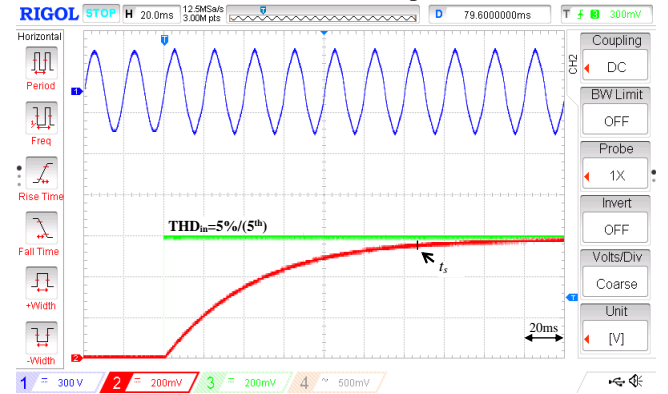


Fig. 17. THD experimental result for grid with a 5<sup>th</sup> harmonic and 5% amplitude sudden step perturbation. Ch. 1: Grid voltage (300V/div). Ch. 2: THD (200mV/div or 1.66%/div). Ch. 3: 5% step reference signal (200mV/div or 1.66%/div).

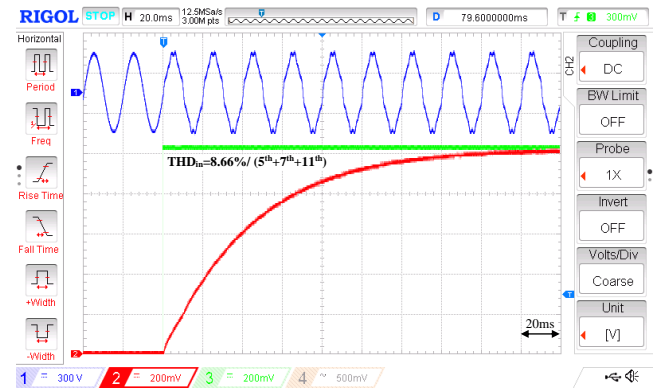


Fig. 18. THD experimental result for grid with a combination of a 5<sup>th</sup>, 7<sup>th</sup> and 11<sup>th</sup> harmonics (5% amplitude each) sudden step perturbation. Ch. 1: Grid voltage (300V/div). Ch. 2: THD (200mV/div or 1.66%/div). Ch. 3: 8.66% step reference signal (200mV/div or 1.66%/div).

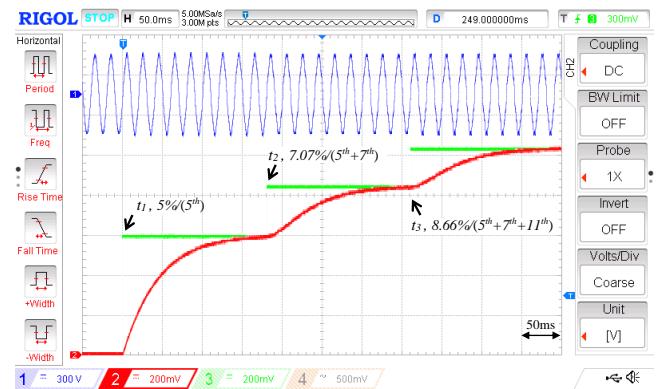


Fig. 19. THD experimental results for sequential perturbations of a 5<sup>th</sup>, 7<sup>th</sup> and 11<sup>th</sup> harmonics that were consecutively activated after 0.21s each. Ch. 1: Grid voltage (300V/div). Ch. 2: THD (200mV/div or 1.66%/div). Ch. 3: Step reference signals, 5% at  $t_1$ , 7.07% at  $t_2=7.07\%$  and 8.66% at  $t_3$  (200mV/div or 1.66%/div).

In the same manner, Fig. 18 shows the experimental result for a simultaneous 5<sup>th</sup>, 7<sup>th</sup> and 11<sup>th</sup> harmonics perturbation of 5% amplitude each, which corresponds to an input THD step perturbation of 8.66%. Note in Fig. 17 and 18 that the THD is close to the expected 5% and 8.66% values. In fact, these THDs reach the steady state values of 4.8% and 8.45%, respectively, which correspond to the expected ones for the



designed  $\zeta$  parameter (see Fig. 5 and 6). The measured settling time in Fig. 18 considering a 2% error criterion regarding the THD steady-state is  $t_s=130\text{ms}$ , which also corresponds to the expected dynamics.

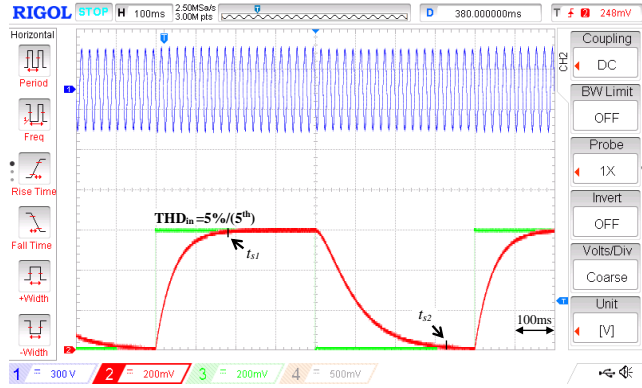


Fig. 20. Experimental results of the THD measurement method for a periodic perturbation of a 5<sup>th</sup> harmonic of 5% amplitude. Ch. 1: Grid voltage (300V/div). Ch. 2: THD (200mV/div or 1.66%/div). Ch. 3: 5% step reference signal (200mV/div or 1.66%/div).

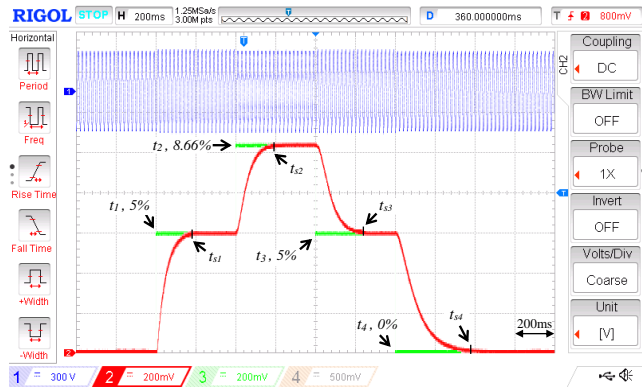


Fig. 21. THD experimental results for sequential THD perturbations using a 5<sup>th</sup>, 7<sup>th</sup> and 11<sup>th</sup> harmonics: from 0 to 5% at  $t_1$ , from 5% to 8.66% at  $t_2$ , back from 8.66 to 5% at  $t_3$  and back from 5 to 0% at  $t_4$ . Ch. 1: Grid voltage (300V/div). Ch. 2: THD (200mV/div or 1.66%/div). Ch. 3: Step reference signals,  $t_1$  &  $t_3=5\%$ ,  $t_2=8.77\%$ , and  $t_4=0\%$  (200mV/div or 1.66%/div).

The SOGI damping factor was reduced to  $\zeta=0.34$  in order to increase the accuracy of the measurement to a 1% error for a 5<sup>th</sup> harmonic using the plots of Fig. 8. A sequence of 5<sup>th</sup>, 7<sup>th</sup> and 11<sup>th</sup> harmonic perturbations of 5% amplitude each were programmed in the AC power source. The 5<sup>th</sup> harmonic happened first at  $t_1$ , followed by a 7<sup>th</sup> harmonic after 0.21s, labeled as  $t_2$ , and by a 11<sup>th</sup> harmonic after 0.42s, labeled as  $t_3$ . Then, the grid had a THD sequence perturbation going to 5%, 7.07% and 8.66%, respectively. Fig. 19 depicts the experimental result, which clearly shows that the THD is accurate. The measured THDs from the inner DSP variables were 4.95%, 7.02% and 8.60%, respectively, which coincide with Fig. 10.

Next, Fig. 20 depicts the result for a periodic perturbation of a single 5<sup>th</sup> harmonic with 5% amplitude in order to see the impact of the square root nonlinear operator in the dynamic response. In Fig. 20 two settling times have been labeled:  $t_{s1}$  and  $t_{s2}$ . Note how  $t_{s2}$ , at the step-down transient, is much larger than  $t_{s1}$ , which denotes the same behavior than explained in section III.C. Moreover, other sequential THD step perturbations were used starting first from 0% to 5% THD using a 5<sup>th</sup> harmonic at  $t_1$ , then from 5% to 8.66% using

additional 7<sup>th</sup> and 11<sup>th</sup> harmonics at  $t_2$ , then back from 8.66% to 5% at  $t_3$  and finally back from 5% to 0% at  $t_4$ . Fig. 21 depicts the experimental response. As seen, the transient responses at  $t_1$  and  $t_2$  have a similar settling time ( $t_{s1}$  and  $t_{s2}$ ). However, the transient at  $t_3$  is a bit larger than the previous ones and the transient at  $t_4$  is visibly the longest one, as illustrated that happens in section III.C.



Fig. 22. THD experimental results to frequency step perturbation from 50Hz to 55Hz. The grid has a permanent 5<sup>th</sup> harmonic distortion with a 5% amplitude. Ch. 1: Grid voltage (300V/div). Ch. 2: THD (200mV/div or 2.5%/div). Ch. 3: Estimated frequency (500mV/div or 5Hz/div).

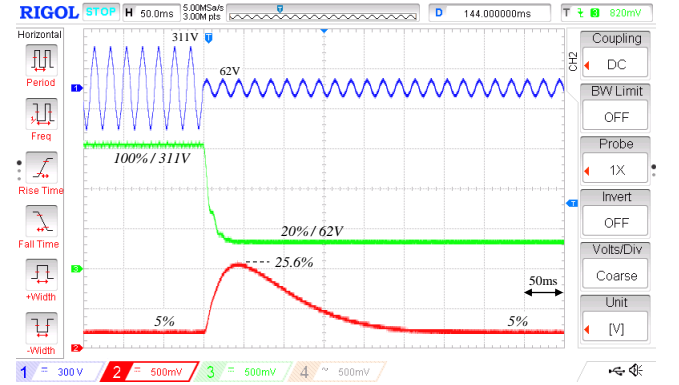


Fig. 23. THD experimental results to 80% depth voltage sag. The grid has a permanent 5<sup>th</sup> harmonic distortion with a 5% amplitude. Ch. 1: Grid voltage (300V/div). Ch. 2: THD (500mV/div or 12.5%/div). Ch. 3: Estimated amplitude voltage (500mV/div or 100V/div).

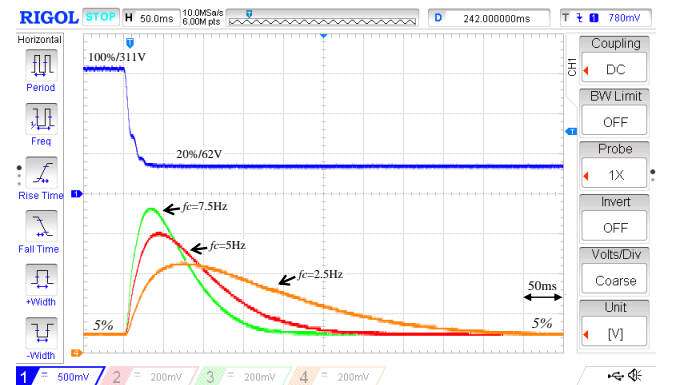


Fig. 24. THD experimental results to 80% depth voltage sag. The grid has a permanent 5<sup>th</sup> harmonic distortion with a 5% amplitude. Ch. 1: Estimated amplitude voltage (500mV/div or 100V/div). Ch. 2, Ch3, Ch4: THD for  $f_c=5\text{Hz}$ , 7.5Hz and 2.5Hz, respectively (200mV/div or 10%/div).

Fig. 22 and 23 depict the response to a frequency step perturbation from 50Hz to 55Hz and to an 80% depth voltage, respectively. The SOGI-FLL and LPF parameters were  $\zeta=0.7$ ,  $\lambda=55\cdot 2\pi 50 \text{ rad/s}^2$ ,  $\zeta=0.34$ ,  $n=2$  and  $f_c=5\text{Hz}$ . Notice in Fig. 22 that the THD peak amplitude regarding 5%

is 3.6% and that the voltage sag in Fig. 23 induces a THD peak amplitude of 26.5%, which coincide with the results showed in Fig. 13 and 14, respectively.

Finally, Fig. 24 shows the results using a LPF with different cutoff frequencies,  $f_c=7.5\text{Hz}$ ,  $5\text{Hz}$  and  $2.5\text{Hz}$  and grid with an 80% depth voltage sag. Note that the results coincide with the obtained in Fig. 15.

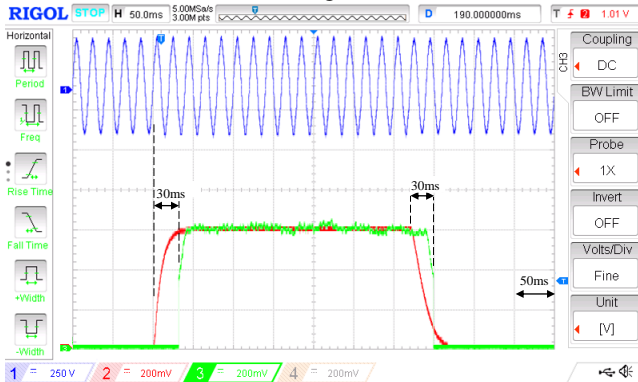


Fig. 25. Experimental results for FFT-based THD ( $N=64$ ) and proposed THD methods for a periodic perturbation of a 5<sup>th</sup> harmonic of 5% amplitude. Ch. 1: Grid voltage (250V/div). Ch. 2: THD (200mV/div or 1.66%/div). Ch. 3: FFT-based THD (200mV/div or 1.66%/div).

### B. Comparison with the FFT-based THD

An alternative online FFT-based THD measurement method was implemented on a second board with a TMS-320F28377D 200MHz DSP with more Ram Capability (172kb). The FFT was computed using the subroutines of the optimized library provided by TI [24]. The FFT can be applied on a digitalized signal with  $N=64, 128, 256, 512,$  or  $1024$  samples per period, and requires of the following memory resources: a  $2N$ -size input buffer for holding a minimum of two periods of the signal, two  $2N$ -size buffers for intermediate variables, an  $N$ -size buffer for coefficients, and an  $(N/2+1)$ -size output buffer to provide the magnitude of the fundamental and harmonics components. The sampling time  $T_s$  is determined as  $T_s=1/(50N)$  s.

The computational burden of the employed FFT routines was measured using a digital output pin of the DSP. The measurements were made considering a 50Hz grid voltage signal and are shown at Table III. The results indicate that the FFT routines can only be applied for  $N=64$  and  $128$ , since only in these cases the time needed to compute the FFT is lower than the required sampling time  $T_s$ . The time needed for  $N=256, 512$  and  $1024$  is higher than  $T_s$  and, thus, the FFT cannot be processed at every sample by the DSP. Therefore, the comparison between the two THD measurement methods will only be made for  $N=64$  and  $N=128$ .

The THD is computed according to (1) in the following order: 1<sup>st</sup>) the FFT routines in [24] are applied once the input buffer is filled with samples of the grid voltage, 2<sup>nd</sup>) the sum of the squares of the harmonics provided at the output buffer is computed using a software loop, 3<sup>rd</sup>) the THD is calculated applying the square root operation and then dividing by the fundamental, 4<sup>th</sup>) the content of the input buffer is displaced one position to leave space for holding the next sample at the next iteration of this process.

The FFT library provides information about the number of processor cycles needed for executing the routines [24]. These data have been used here for estimating the burden required to compute the FFT-based THD, which is given in Table IV. This table also shows the number of 32-bit floating

point RAM variables required for the computation. In the same way, the computational burden of the proposed THD method following the schemes depicted in Fig. 2 and Fig. 4 has been measured, using the Concerto DSP board and the tools of Code Composer Studio software [25]. The results are listed in Table V and show that the computational burden for the proposed THD method is

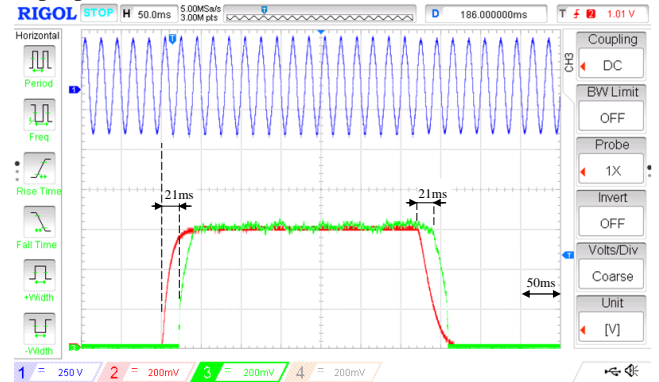


Fig. 26. Experimental results for FFT-based THD ( $N=128$ ) and proposed THD methods for a periodic perturbation of a 5<sup>th</sup> harmonic of 5% amplitude. Ch. 1: Grid voltage (250V/div). Ch. 2: THD (200mV/div or 1.66%/div). Ch. 3: FFT-based THD (200mV/div or 1.66%/div).

Table III. Sampling time  $T_s$  and measured computation time for the FFT-based THD, according to the number of samples  $N$ .

N	64	128	256	512	1024
$T_s$ ( $\mu\text{s}$ )	312.5	156.25	78.12	39.06	19.53
Computation time ( $\mu\text{s}$ )	25.2	50	102.2	214	454

Table IV. Computational burden in processor cycles (c) for the FFT-based THD.

N	64	128
FFT routines (c)	2780	5926
Sum of squares of harmonics (c)	236	460
Square root and division (c)	68	68
Buffer displacement (c)	261	517
<b>Total (c)</b>	<b>3393</b>	<b>7019</b>
<b>Number of 32-bit float RAM variables</b>		
Input buffer	128	256
Output buffer	64	128
Coefficients buffer	64	128
Magnitude buffer	33	65
Other	4	4
<b>Total</b>	<b>293</b>	<b>581</b>

Table V. Computational burden in processor cycles (c) for the proposed THD method.

Block description	Cycles (c)
SOGI	149
$A^2$ and saturation	24
FLL	49
$e^2$ , division and multiplication by 2	32
Square root and multiplication by 100	35
Second-order LPF	65
<b>Total</b>	<b>354</b>
<b>Number of 32bit float RAM variables</b>	<b>29</b>

considerably lower than the FFT-based one and needs of fewer RAM memory resources. The time required for computing the proposed THD method has also been measured and amounts to  $4.3\mu\text{s}$ .

The comparison between the FFT-based THD and the proposed THD measurement method is made for the detection of a periodic 5<sup>th</sup> harmonic distortion. In the test, the cutoff frequency of the THD LPF is chosen as  $f_c=20\text{Hz}$ . Fig. 25 and Fig. 26 depict the results for  $N=64$  and  $N=128$ , respectively.

As can be seen in Fig. 25 and 26, the transient response of the FFT-based THD has a delay that is different in each case. In Fig. 25, for  $N=64$ , the delay is 30ms and in Fig. 26, for  $N=128$ , the delay is 21ms. Therefore, the proposed THD

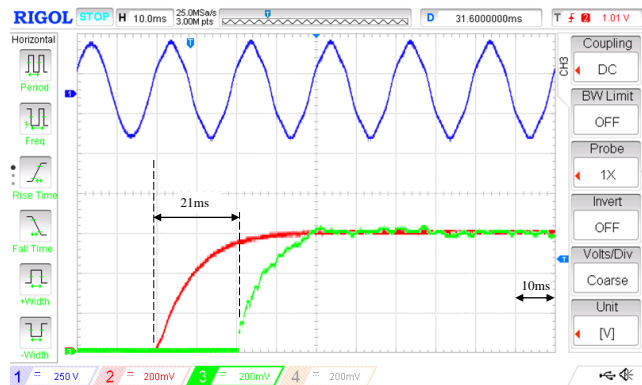


Fig. 27. Detailed (10ms/div) experimental results for FFT-based THD ( $N=128$ ) and proposed THD methods for a periodic perturbation of a 5<sup>th</sup> harmonic of 5% amplitude. Ch. 1: Grid voltage (250V/div). Ch. 2: THD (200mV/div or 1.66%/div). Ch. 3: FFT-based THD (200mV/div or 1.66%/div).

method shows to be faster and less sensitive to noise than the FFT-based one. Fig. 27 shows another scope capture as in Fig. 26 but with more detail (10ms/div). Moreover, the response can be accelerated by increasing the LPF cutoff frequency but at the expense of extra-noise at the THD measurement. Note also that the FFT for  $N=128$  has less noise than for  $N=64$ , which is a general characteristic of the FFT routine, that achieves more accuracy with the increase in the number of signal samples.

Furthermore, the computation of the FFT provides inaccurate results when  $T_s$  deviates from its specified value or when the grid frequency moves away from the nominal frequency. This situation has been programmed and tested in the experiments, showing problems only in the FFT-based THD method. Fig. 28 and 29 show the comparative results for the FFT-based THD for  $N=64$  and 128, respectively, when the operating grid frequency is 51Hz. Notice in these last two figures that the FFT-based THD measurement method is always inaccurate and provides results with nonlinear oscillations and DC-offset errors. Moreover, the greater the frequency deviation, the more the inaccuracy in the THD measurement increases. Note that for the proposed THD method this problem does not exist.

In summary, the proposed THD method is more accurate, requires few computational resources, achieves faster results and has less problems than the FFT-based THD. This points out to its viability for measuring the THD and for being implemented in standard and low cost DSP processors in the different kind of applications suggested at the introduction section of this paper. However, it is important to remark that the method needs of the use of LPF filters to establish clear lower (subharmonic) and higher (maximum harmonic to be considered) boundaries to the input signal. These filters are important to avoid the effect of subharmonics and of extra switching noise in the measurement.

This paper proposes a simple method for obtaining the THD of the grid with a small computational burden requiring of few math operations, a LPF and a square root that can be easily implemented into some standard and low cost DSP processors. The THD is computed using the SOGI-FLL approach that provides the fundamental and harmonic components, but can also be implemented with other grid monitoring solutions like PLL or ANF. The fundamental component amplitude is obtained in this case from the SOGI

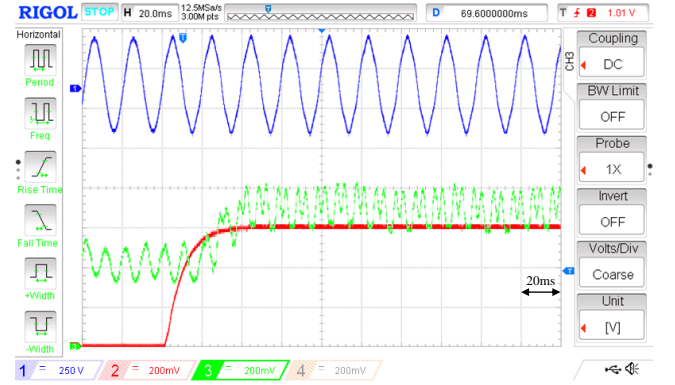


Fig. 28. Experimental results for FFT-based THD ( $N=64$ ) and proposed THD methods for 51Hz grid frequency and a periodic perturbation of a 5<sup>th</sup> harmonic of 5% amplitude. Ch. 1: Grid voltage (250V/div). Ch. 2: THD (200mV/div or 1.66%/div). Ch. 3: FFT-based THD (200mV/div or 1.66%/div).

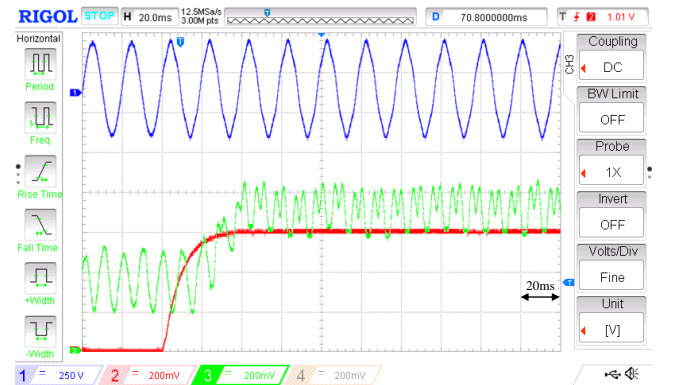


Fig. 29. Experimental results for FFT-based THD ( $N=128$ ) and proposed THD methods for a 51Hz grid frequency and a periodic perturbation of a 5<sup>th</sup> harmonic of 5% amplitude. Ch. 1: Grid voltage (250V/div). Ch. 2: THD (200mV/div or 1.66%/div). Ch. 3: FFT-based THD (200mV/div or 1.66%/div).

orthogonal outputs and the harmonic components through the NF transfer function behavior of the SOGI error signal. The accuracy of the system was analyzed and it was concluded that it relies mainly on the NF capability of the SOGI filter, which is determined by the SOGI damping factor parameter. The THD dynamic response corresponds predominantly to that of the LPF and is determined by its cutoff frequency  $f_c$ . However, the dynamic is affected by the nonlinearity of the square root operator in the THD, which impact the dynamic response with asymmetric effects in the step-up and step-down transient responses. The worst case effects happen at the step-down transient response, when the THD is small and close to zero. The behavior of the method in front of grid perturbations, such as frequency steps and voltage sag perturbations, was also analyzed. These perturbations induce a burst of impulses at the THD input that is filtered out by the LPF, and generate an impulse-like perturbation. This impulsive perturbation disappears after a short time determined by the magnitude of the perturbation

and by the LPF design parameters. Simulations and experimental results were provided that corroborate the performance of the system in terms of accuracy, dynamic response and robustness in front of grid perturbations. Moreover, an experimental comparison with a FFT-based THD is made, showing that the proposed method is faster and has a very small computational burden regarding the FFT one. Additionally, the proposed THD method provides a measurement with less noise and is robust in front of grid frequency variations from nominal frequency.

#### REFERENCES

- [1] R. C. Dugan, M. F. Mcgranaghan, S. Santoso, and H. W. Beaty. *Electrical Power Systems Quality*, Third Edition, McGraw-Hill Comp., Inc. 2002.
- [2] A. Kusko and M.C. Thompson. *Power quality in electrical systems*. McGraw-Hill Comp., Inc. 2007.
- [3] IEEE Std 519-1992, "IEEE recommended practices and requirements for Harmonic Control in Electric Power Systems," *Institute of Electrical and electronics engineers, Inc.* 1993.
- [4] G.E. Mog and E.P. Ribeiro, "Total harmonic distortion calculation by filtering for power quality monitoring," *IEEE Transm. and Distr. Conf. and Exp.: Latin Am.*, pp. 1-4, 2004.
- [5] D. Schmilovitz, "On the definition of total harmonic distortion and its effect on measurement interpretation." *IEEE Trans. on Power Delivery*, vol. 20, no.1, pp. 526–528, Jan 2005.
- [6] I.V. Blagouchine and E. Moreau, "Analytic method for the computation of the total harmonic distortion by the Cauchy method of residues," *IEEE Trans. on Commun.*, vol. 59, No. 9, Sept. 2011.
- [7] C. Muresan, F. Dragan and V.D Zaharia, "Total harmonic distortion computation in nonsynchronized sampling condition," *Acta Electrotehnica*, vol. 52, no. 2, pp. 114-118, 2011.
- [8] R. Ingale, "Harmonic analysis using FFT and STFT," *Int. J. of Sig. Process. and Pat. Recogn.*, vol. 7, No. 4, pp. 345-362, 2014.
- [9] N. Farokhina, H. Vadizadeh, S.H. Fathi, and F. Anvariasl, "Calculating the formula of line-voltage THD in multilevel inverter with unequal dc sources," *IEEE Trans. on Ind. Electr.*, vol. 58, no. 8, pp. 3359-3372, Aug. 2011.
- [10] B.M. Antic, Z.L. Mitrovic, and V.V. Vujcic, "A method for harmonic measurement of real power grid signals with frequency drift using instruments with internally generated reference frequency," *Measurement Sci. Review*, vol. 12, no. 6, pp. 277-285, 2012.
- [11] K. Sajjad, G. Kalsoom, and A. Mughal, "Simplified THD measurement and analysis for electronic power inverters," *In Proc. of the IEEE Int. Conf. on Appl. Sci. and Tech. IBCAST'15*, pp. 186-191, 2015.
- [12] R. Abdikarimuly, Y.L. Familiant, A. Ruderman, and B. Reznikov "Calculation of current total harmonic distortion for a single-phase multilevel inverter with LCL-filter," *In Proc. of IEEE Int. Power Electr. and Motion Contr. Conf., PEMC'2016*, pp. 63-68, 2016.
- [13] F.C. Alegria, "Precision of the sine fitting-based total harmonic distortion estimator," *Metrol. and Meas. Syst.*, vol. 23, no. 1, pp. 37-46, 2016.
- [14] D. Yazdani, A. Bakhshai, and P. K. Jain, "A three-phase adaptive notch filter-based approach to harmonic/ reactive current extraction and harmonic decomposition," *IEEE Trans. Power Electron.*, vol.25, no.4, pp.914–923, Apr. 2010.
- [15] B. Burger and A. Engler, "Fast signal conditioning in single phase systems," *in Proc. of Eur. Pow. Electr. Conf., EPE'01*, 2001.
- [16] P. Rodriguez, A. Luna, M. Ciobotaru, R. Teodorescu, and F. Blaabjerg, "Advanced grid synchronization system for power converters under unbalanced and distorted operating conditions," *in Proc. IECON'06*, pp. 5173-5178, 2006.
- [17] J. Matas, M. Castilla, J. Miret, L. G. de Vicuna, and R. Guzman, "An adaptive prefiltering method to improve the speed/accuracy tradeoff of voltage sequence detection methods under adverse grid conditions," *IEEE Trans. Ind. Electron.*, vol. 61, no. 5, pp. 2139–2151, May 2014.
- [18] J. Matas, H. Martin, J. de la Hoz, A. Abusorrah, Y. Al-Turki, and M. Al-Hindawi, " A Family of Gradient Descent Grid Frequency Estimators for the SOGI Filter," *IEEE Trans. Power Electron.*, vol. pp. no. 99, 2017.
- [19] M. Ciobotaru, R. Teodorescu, and F. Blaabjerg, "A New Single-Phase PLL Structure Based on Second Order Generalized Integrator," *IEEE Power Elect. Special. Conf., PESC'06*, pp. 1-6, 2006.
- [20] M. Karimi-Ghartemani and M. R. Iravani, "A nonlinear adaptive filter for online signal analysis in power systems applications," *IEEE Trans. Power Del.*, vol. 17, no. 2, pp. 617–622, Apr. 2002
- [21] M. Karimi-Ghartemani, *Enhanced Phase-Locked Loop Structures for Power and Energy Applications*. Piscataway, NJ, USA. IEEE Press, 2014.
- [22] S. Golestan, J.M. Guerrero, and J.C. Vasquez, "Single-phase PLLs: a review of recent advances," *IEEE Trans. Power Electron.*, vol. 32, no. 12, pp. 9013-9030, Dec. 2017.
- [23] S. Golestan, E. Ebrahimzadeh, and J.M. Guerrero, and J.C. Vasquez, "An Adaptive Resonant Regulator for Single-phase Grid-Tied VSCs," *IEEE Trans. Power Electron.*, vol. pp. no. 99, 2017.
- [24] *FPU DSP Software Library User's Guide*, Texas Instruments, 2015.
- [25] *Code Composer Studio Users Guide*, Texas Instruments, 2019. [Online]. Available: <http://www.ti.com/tool/CCSTUDIO>